Pergamon

0301-9322(93)E0006-Q

Int. J. Multiphase Flow Vol. 20, No. 1, pp. 117–129, 1994

0301-9322/94 $6.00 + 0.00

PARTICLE WAKE EFFECTS ON THE DRAG FORCE OF AN INTERACTIVE PARTICLE

C. ZHU, S.-C. LIANG and L.-S. FAN†
Department of Chemical Engineering, Ohio State University, Columbus, OH 43210, U.S.A.

(Received 11 February 1993; in revised form 10 October 1993)

Abstract—Direct measurements of the drag force on two interacting particles arranged in the longitudinal direction for particle Reynolds numbers (Re) varying from 20 to 130 are conducted using a microforce measurement system. The system is capable of measuring the force up to 50 g with an accuracy of 1 mg. The effects of the interparticle distance and Re on the drag forces of both the trailing and leading particles are examined. An empirical equation is obtained to describe the drag force variation of a single particle trailing in the wake of a leading particle. A mechanistic model is also developed to account for the motion of the trailing particle in the wake region of the leading particle as well as for their contact velocity. Moreover, a simultaneous flow-field visualization is conducted to characterize the wake flow phenomena. The results indicate that Re affects not only the magnitude of the drag force of an interacting particle but also its variation with the interparticle distance. At contact, the drag force of a trailing particle can be less than one-fifth of the drag force of a single particle without interparticle effects. Both the drag force measurements and the flow-field visualization reflect that the wake-influenced region of the leading particle can be longer at a lower Re. The mechanistic model suggests that both the drag force and the Basset force should be included in the description of the motion of the trailing particle in the wake region of the leading particle. The model predicting the contact velocity of the two particles is reasonably validated with the experimental data.

Key Words: drag force, particle interaction, wake effects, particle–particle contact velocity

1. INTRODUCTION

The description of the general motion of various phases in a multiphase flow system requires information regarding the drag forces between the phases. Except for a very dilute system, where individual particle motion can be treated independently, the effect of fluid-dynamic interactions between particles on the drag force cannot be neglected. The fundamental understanding of the effect of the fluid-dynamic interactions on the drag force relies on the direct and accurate measurements of this force. The particle Reynolds numbers (Re) based on the single-particle terminal velocity and the particle diameters are less than several hundreds for most applications in multiphase flows. For example, at Re = 10 to 200, the corresponding sizes of glass beads vary from 230 μm to 1.1 mm in water and from 130 to 650 μm in air. Hence, the study of drag forces of interacting particles in the low Re range (less than several hundreds) is of practical significance.

Theoretical work on the drag force of interacting particles is limited to very low Re (mostly for creeping flows), due to the nonlinearity of the equations governing the flow motion at higher Re. The only multiparticle system for which the drag force can be rigorously determined analytically is a two-particle system. For systems with more than two particles, it is unlikely one will find a coordinate system to simultaneously satisfy all the boundary conditions. Stimson & Jeffery (1926) employed a bipolar coordinate system to solve the velocity field of a slow-moving fluid flowing around two equal-sized particles aligned in the flow direction. For flow systems with more than two particles, the method of reflection is usually used. So far, no theoretical studies have been reported in the intermediate Re region for multiparticle flows.

Pioneering studies on direct measurements of the drag forces of interacting particles were conducted by Rowe & Henwood (1961), Lee (1979) and Tsuji *et al.* (1982). Lee (1979) measured the drag force of an interacting particle at Re $\approx 10^4$. Rowe & Henwood (1961) and Tsuji *et al.* (1982) attempted to measure the drag force at Re $< 10^3$. Both of them used the "pendulum method" and

†To whom all correspondence should be addressed.

water channel flow to measure the drag force directly; however, limited by the approaches, their data were so scattered that these data could only reflect a general trend of the interactions. For $Re < 200$, no reliable quantitative results of the drag force of a particle under the influence of other particles are available. Thus, the effect of Re on the drag force in this Re range needs to be explored.

Joseph (1993) described the particle–particle interactions in terms of "drafting", "kissing" and "tumbling". The interpretation of this phenomenon can be closely associated with the variation of the drag force of the interactive particles. The "drafting" and "kissing" occur once a trailing particle is trapped in the wake region of a leading particle. The trailing particle will be accelerated, due to the wake attraction, and soon catches up with the leading particle at a certain contact velocity. This phenomenon, from a microscopic point of view, in effect reveals one of the basic mechanisms of the unsteady and transient nature of particulate flows. However, quantitative descriptions of such acceleration or mechanistic models are not available, partly due to the lack of information on the drag force under the influence of other particles.

The drag force of a single particle in a uniform flow can be written in terms of Re as

$$f_{d0} = C_{D0} \frac{\pi}{8} \frac{\mu^2}{\rho} \mathrm{Re}^2, \qquad [1]$$

where f_{d0} is the drag force, Re is the particle Reynolds number, C_{D0} is the drag coefficient (which is a function of Re) and μ and ρ are the fluid viscosity and density, respectively. Use of water as a working fluid would lead to a range of f_{d0} between 0.012–1.1 mg when Re varies from 10 to 200. It is acknowledged that the variation in the drag force in such a force range is too small to be detected accurately. Equation [1] indicates, however, that the drag force at a given Re number is proportional to μ^2. Thus, using a fluid of high viscosity could augment the drag force to an accurately detectable range.

In the present experimental study, a mixture of glycerin and water is used. The viscosity is adjusted to vary from 0.03 to 0.1 kg/m-s by altering the concentration of glycerin as well as the fluid temperature. Hence, the resulting drag force range is significantly increased to a range from 30 mg to 11 g. The variations in the drag forces of interacting particles with the distance between the two particles can thus be measured and correlated.

The flow structure in the particle wake region is also studied to investigate the basic flow field under the influence of particle–particle interactions. Taneda (1979) presented excellent pictures on the flow field around two particles at $Re < 20$, mostly in the creeping flow regime. In this low Re region, he observed flow separation around the spheres at small interparticle distances and the formation of vortex rings in the area between two particles. By use of the flow visualization technique, Tsuji *et al.* (1982) discussed the configuration and dynamics of the vortices of two spheres co-aligned with the flow for $Re > 200$. In the current study, the flow visualization is focused on the wake-influenced region between two interacting particles in the Re range 30–130.

To quantify the drag force effect associated with the particle–particle interactions in a gas–solid flow, the motion of a trailing particle in the wake of a leading particle as well as their contact velocity is simulated in this study by a mechanistic model. In this simulation, the drag force is represented by an empirical equation based on the present measurements. Due to the relative acceleration between the two particles, the equation of motion for the trailing particle also incorporates carried mass and Basset force effects. The predicted contact velocity based on the present model is validated with the experimental data.

2. EXPERIMENTAL APPARATUS AND MEASUREMENT SYSTEMS

The experimental setup is shown in figure 1. It consists of a circulating loop, a drag force measuring system and a flow visualization and velocity measuring system. The circulating fluid is a glycerin–water mixture with glycerin ranging from 75 to 85 wt%. The temperature of the fluid is maintained constant in each run of the experiments. For different runs, the temperature varies from 17 to 23°C to achieve the desired fluid viscosities. The fluid viscosity is measured by a rotational viscometer (Fann series 35 viscometer). Over this temperature range, the fluid viscosity varies from 0.03 to 0.1 kg/m-s. The flow is circulated continuously through a vertical cylindrical column of 10.16 cm i.d. A larger expanded region is used to disengage the fluid, thus minimizing

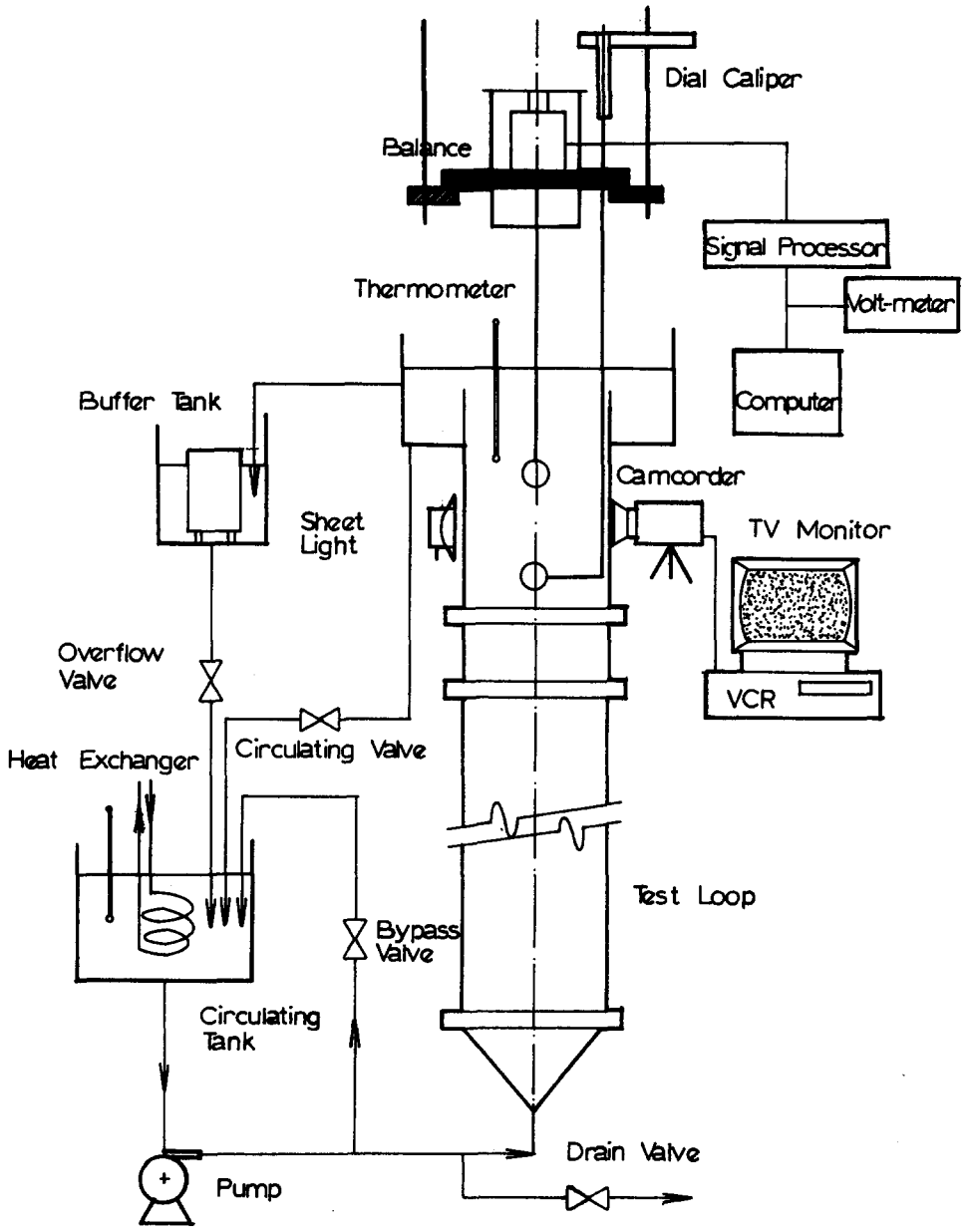

Figure 1. Schematic diagram of the experimental setup.

the end effect of the column on the test particles. Brass balls of 1.587 cm dia are used as test particles. By changing the fluid velocity and viscosity, Re varies from 20 to 130.

A top-loading electronic balance with a sensitivity of 1 mg (Scientech, model 202-004) is used to measure the drag force. In order to lower the vibration noise on the balance during the experiments, the balance is anchored onto the ceiling so that the support of the microforce measuring system is separated from that of the circulating loop. The analog output is converted to a digital signal through an A/D board with 16-bit resolution (National Instruments data acquisition board AT-MIO-16x). The data sampling frequency is 100 Hz. The time-averaged value is obtained over a time period of 20 s. As shown in figure 2, two different arrangements of the test particles are used in this study. These two arrangements allow the measurement of the drag force of either the trailing particle [figure 2(a)] or the leading particle [figure 2(b)]. Note that the particle at the lower elevation (upstream) is denoted as the leading particle and the other as the trailing particle. The rigid rod support is made as short as possible to minimize the vibration induced by

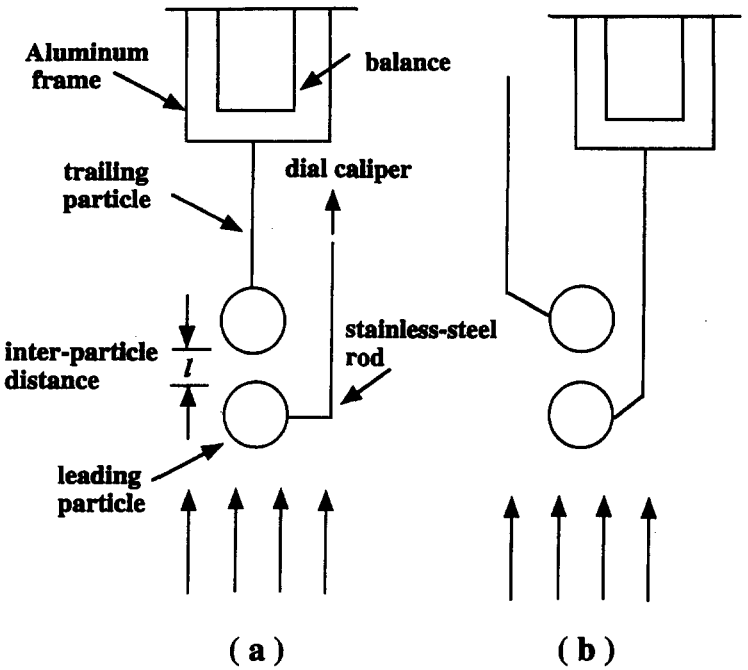

Figure 2. Two arrangements of the test particles to study the drag force of (a) the trailing particle and (b) the leading particle.

the flow. The interparticle distance l/d is measured by use of a dial caliper with an accuracy of 0.0254 cm. The particles are placed along the centerline of the test column.

The total drag force on the test particle and its supporting rods is obtained by deducting the gravitational and buoyancy contributions from the total force measured by the balance. The gravitational and buoyancy forces are predetermined in the stationary fluid. For both particle arrangements shown in figure 2, the drag force on the 0.16 cm dia rod is measured in the same manner and in the same flow field as used for the drag forces of the particles. It is noted, however, that in measuring the drag force of the rod, there is no direct attachment of the particle to the rod. With the drag force on the rod predetermined, the drag on the particle can be obtained by simply subtracting the drag on the rod from the combined drag. Thus, the drag coefficient of the particle can be calculated from [1].

For both the flow visualization and velocity measurements, a collimated light sheet is created to illuminate the center plane of the test section. Due to the high viscosity of the fluid, tiny bubbles are inherently present in the flow stream; these bubbles serve as flow tracers. The size of these

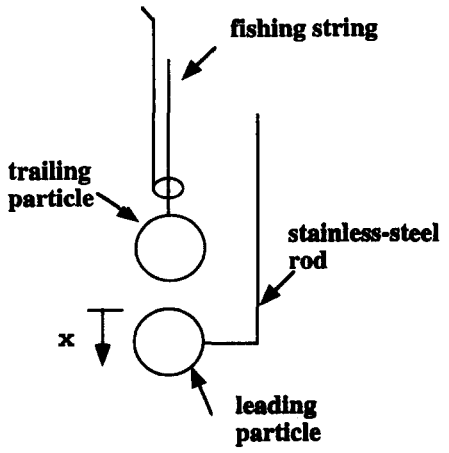

Figure 3. Particle arrangement for the particle–particle contact velocity experiments.

bubbles is of the order of 100 μm. Thus, the relative velocity between the bubbles and the fluid is negligibly small (about 0.1% of the fluid velocity). A video system is used to track the local flow information around the test particles. The flow velocity is determined by tracking the motion of the tiny bubbles.

The measurements of the particle–particle contact velocity are carried out in the same Re range. The procedure involves adjusting the flow velocity in the central region to match the terminal velocity of the test particles. To assure this condition is met, the trailing particle hung by a fishing string is confirmed as remaining still in the center region. The leading particle is fixed in the center of the column. A thin rod with a hook on one end is used to adjust the position of the trailing particle, as shown in figure 3. At a distance where wake attraction just prevails, the trailing particle is released. The entire motion of the trailing particle from its release to contact with the leading particle is recorded on a video tape. In these measurements, the particles used are hollow polypropylene (PP) balls of 1.9 cm dia. The density of the PP particle is adjusted by filling in with fluids of different densities to arrive at the desired terminal velocity.

3. DRAG FORCE MEASUREMENT—RESULTS AND DISCUSSION

3.1. Drag forces under longitudinal interaction of two particles

Since the ratio of the particle diameter, d, to the column diameter, D, employed is about 0.15, the flow is laminar when $Re < 200$. Thus, the flow field around the particles can be reasonably regarded as uniform. It is found that in all the experimental conditions, the drag force of the supporting rod contributes 30–40% of the total measured drag force on the particle–rod system. The drag force measurement system is validated by comparing the drag coefficient of a single particle with that reported in the literature (Schlichting 1979). As shown in figure 4, the agreement is reasonable with an error margin of $<5\%$.

Typical results of the drag of the trailing particle under the influence of the leading particle at various Re values are illustrated in figure 5. The drag force is nondimensionalized by the drag force of a single noninteracting particle under the same Re. The interactive distance, l, is also expressed in a dimensionless form, l/d. Figure 5 shows that the drag ratio of the trailing particle decreases exponentially with decreasing l/d and reaches a minimum at the contact position, which agrees with the results of Rowe & Henwood (1961) and Tsuji *et al.* (1982). The reduction in the drag ratio is caused by the wake effect. Moreover, in both Rowe & Henwood's and Tsuji *et al.*'s experiments,

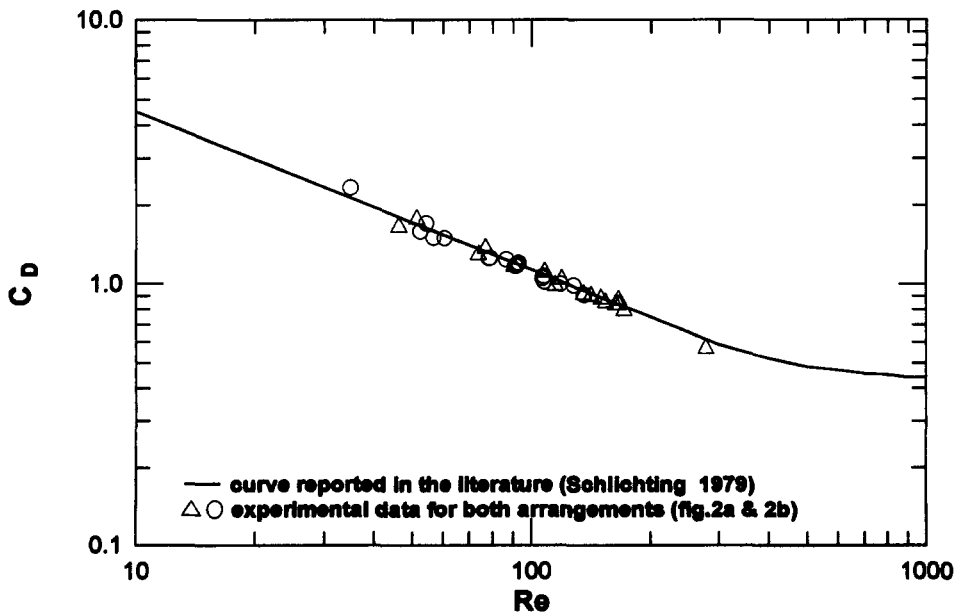

Figure 4. Comparisons of the experimental drag coefficient of a single noninteracting particle with that from the literature.

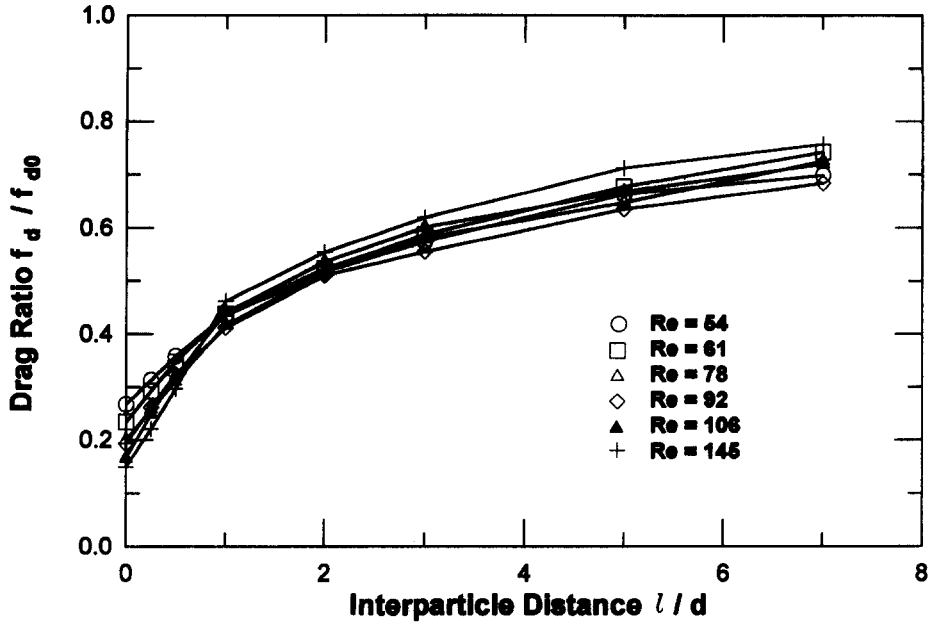

Figure 5. Experimental data for the variation in the drag ratio with the interparticle distance.

the data were scattered and the drag ratio was shown to be insensitive to the change of Re. In this study, however, it is found that the change in the drag ratio depends significantly on Re as well as the interactive distance. Further comparisons of the experimental data with those reported by Rowe & Henwood (1961) and Tsuji *et al.* (1982) show that the data agree well quantitatively in the same Re range. For the case where two particles closely contact with each other, the drag ratio decreases with an increase in Re. The values of the drag ratio under near-contact conditions in the Re range studied are smaller than the value of 0.645 for the Stokes region (Happel & Brenner 1965), indicating that the change in the drag ratio with the Re is in a correct trend. It is also found that the curves for different Re may cross each other at l/d of about 1–3. At a small l/d, the drag ratio of a higher Re decreases faster within the Re range tested.

An empirical relation is obtained to describe both effects of the interparticle distance l/d and Re on the dimensionless drag of the trailing particle. The empirical equation takes the exponential form

$$\frac{f_d}{f_{d0}} = 1 - (1 - A)\exp\left(B\frac{l}{d}\right), \qquad [2]$$

where f_d is the drag force of an interactive particle and f_{d0} is the drag force of a single noninteracting particle. The coefficients A and B are both functions of Re and are empirically correlated as

$$A = 1 - \exp(-0.483 + 3.45 \times 10^{-3}\,\mathrm{Re} - 1.07 \times 10^{-5}\,\mathrm{Re}^2) \qquad [3a]$$

and

$$B = -0.115 - 8.75 \times 10^{-4}\,\mathrm{Re} + 5.61 \times 10^{-7}\,\mathrm{Re}^2. \qquad [3b]$$

It is noted that the application of [3a, b] should be limited to $20 < \mathrm{Re} < 150$.

Equation [2] is examined at two limits of the separation distances between the two particles. As $l \to \infty$, the second term in [2] vanishes and the drag ratio becomes unity as expected. At contact, the drag ratio equals the coefficient A, which gives the minimum value of the drag ratio. The crossing phenomena are also simulated by [2] and [3], as shown in figure 6. It should be mentioned that the correlation proposed by Rowe & Henwood (1961) was in a hyperbolic form. This is invalid for small interparticle distances since the drag ratio approaches either positive or negative infinity at contact.

As shown in figure 7, the drag of the leading particle is almost unchanged by the approach of the trailing particle. This result agrees with the measurements of Rowe & Henwood (1961) and

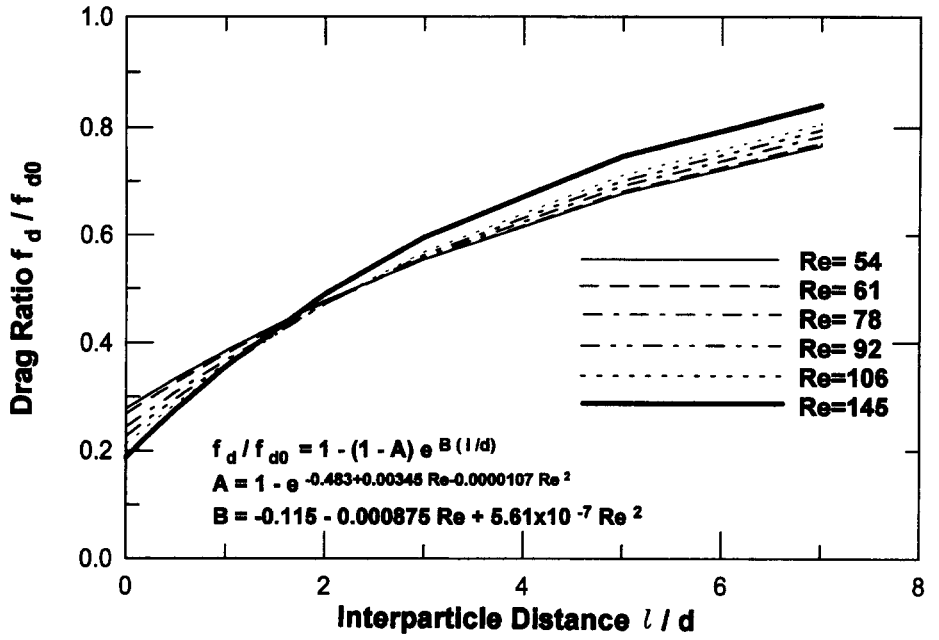

Figure 6. Calculated results based on the empirical equation for the variation in the drag ratio with the interparticle distance.

Tsuji *et al.* (1982). It is noted that there is a small decrease in the drag ratio around $l/d = 1$. Thus, comparing figure 5 and figure 7, it can be concluded that the influence of the leading particle on the drag force of the trailing particle is significantly larger than that of the trailing particle on the leading particle.

3.2. Flow-field visualization

Figures 8(b–d) illustrate the typical flow patterns in the wake-influenced region between two interacting particles for several interparticle distances l/d at $Re = 90$. For comparison, the wake

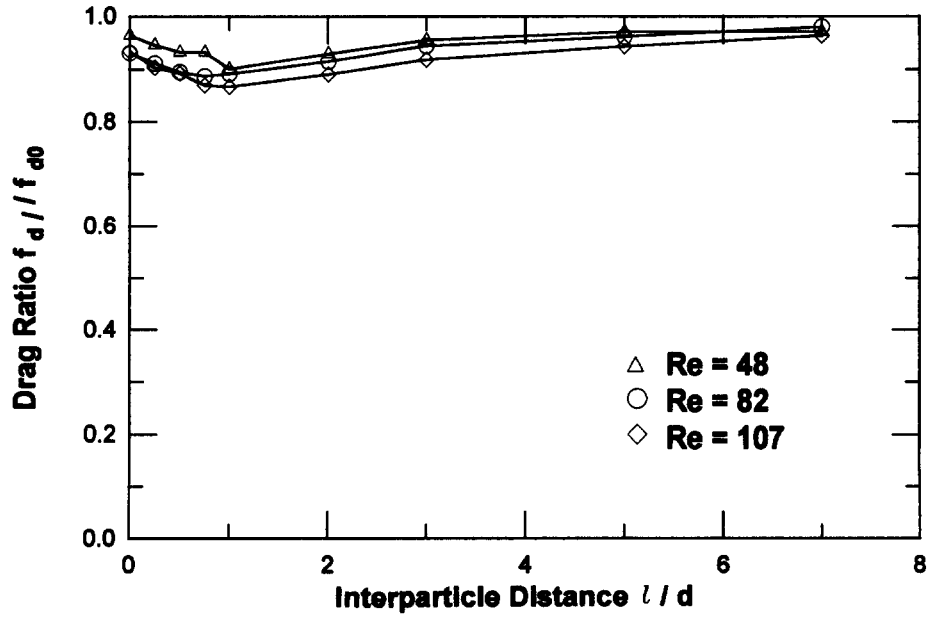

Figure 7. Variation in the drag ratio of the leading particle with the interparticle distance at two Re values.

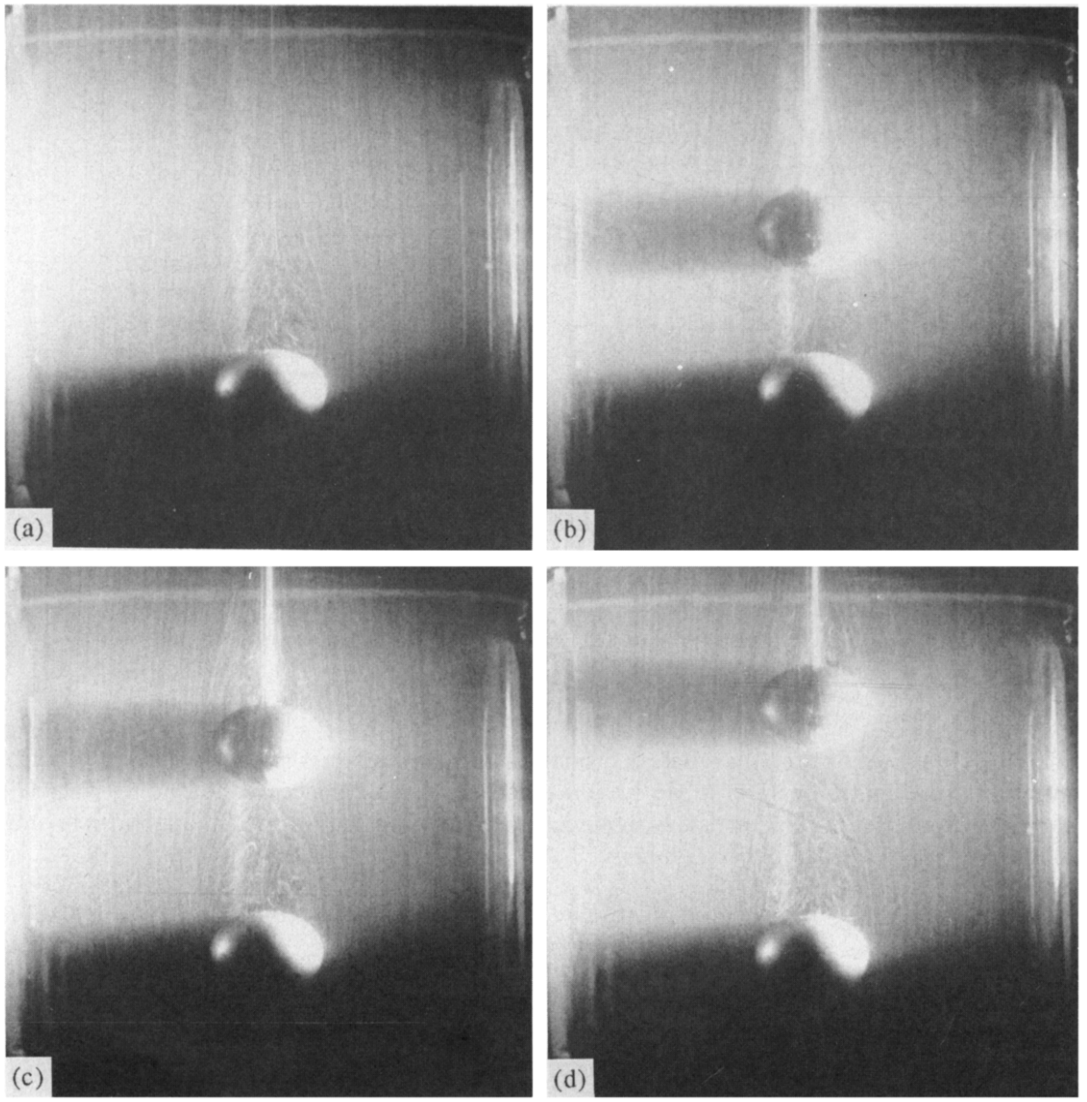

Figure 8. The flow field between two particles: (a) a single particle; (b) $l/d = 1$; (c) $l/d = 1.5$; (d) $l/d = 2$.

behind a single noninteracting particle is also shown in figure 8(a). It is observed that when the trailing particle is placed 1 particle diameter away from the leading particle, the wake vortex does not end at a distance of 0.9 particle diameter as it would be for a single noninteracting particle. When l/d is increased to 1.5, the wake vortex still does not end completely. This indicates that the wake-influenced region is significantly extended due to the presence of the trailing particle. At a distance of 2 particle diameters, the wake vortex of the leading particle appears to have the similar structure to that of a single noninteracting particle, albeit elongated. Figure 9 shows another phenomenon where the wake-influenced region at a higher Re is extended more than at a lower Re. The crossing phenomena may have close bearings with this observation. The Re in figures 9(a) and 9(b) are 80 and 44, respectively. The l/d in these two cases are about 2 particle diameters.

4. PARTICLE MOTION DUE TO WAKE ATTRACTION

The acceleration of a particle due to wake attraction is of particular significance as it reveals one of the basic mechanisms of the unsteady and transient nature of particulate flow. Information on the particle–particle contact velocity, as a result of such acceleration, is essential to the quantification

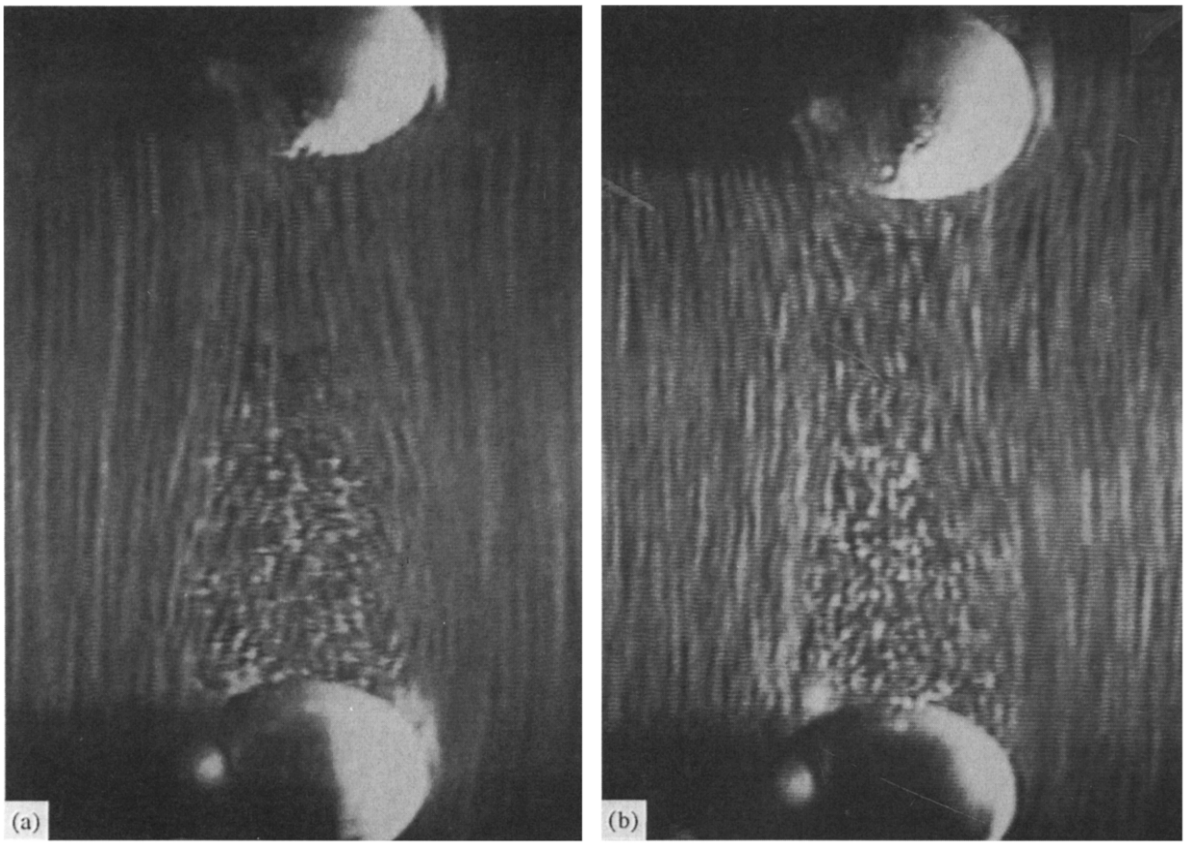

Figure 9. The wake-influenced region between two particles: (a) Re = 80; (b) Re = 44.

of the momentum transfer due to collisions among particles. Based on the experimental results, a simple mechanistic model is developed to describe the motion of a particle due to wake attraction. To validate this model, the predicted contact velocity are compared with the experimental data. The comparisons indicate that both the drag force and the Basset force should be included in the equation describing of the motion of a trailing particle in the wake region of a leading particle.

4.1. Model

Three basic assumptions have been made in the development of this model: (1) the motion of the leading particle is not affected by the approach of the trailing particle; (2) particles are equal-sized, rigid and spherical; (3) initially, both particles move at their terminal velocity and are separated by a characteristic distance. The origin of the coordinate is selected on the top edge of the leading particle. The axis is chosen in the opposite direction of the upstream flow, as shown in figure 3. In this model, four different forces—namely the gravitational force, the buoyancy force, the drag force and the Basset force—are considered to account for the motion of the trailing particle. The drag force term is modified by the proposed empirical equation. The original form of the Basset force is used to describe the acceleration history of the particles, although it is obtained for the creeping flow condition. There have been many modifications of the Basset force outside the Stokes region, such as those suggested by Odar & Hamilton (1964) and Clift *et al.* (1978). Most of the modified forms were obtained by simply multiplying a factor with the basic form of the Basset integral and were based on simple harmonic oscillating flows where the information of the tracking history of the acceleration is missing. Therefore, in the present model, the original form of the Basset integral is used as a first-order approximation of the Basset force.

During the acceleration process, a single particle also experiences a force due to the inertia of the surrounding fluid, i.e. the added mass. For a spherical particle, the added mass is equal to one-half of the mass of the fluid displaced by the particle. Hence, a general momentum equation takes the form:

$$(\rho_p + \tfrac{1}{2}\rho)V\frac{dU}{dt} = (\rho_p - \rho)Vg - f_d - f_B, \quad [4]$$

where ρ_p is the particle density, ρ is the fluid density, V is the volume of the particle, f_d is the drag force and f_B is the Basset force. The Basset force f_B is approximated by

$$f_B = \tfrac{3}{2}d^2\sqrt{\pi\rho\mu}\int_0^t \frac{\dfrac{dU}{d\tau}}{\sqrt{t-\tau}}\,d\tau. \quad [5]$$

Based on assumption (3), the drag force of a single noninteracting particle f_{d0} is given as

$$f_{d0} = (\rho_p - \rho)Vg. \quad [6]$$

Note that the drag force of the trailing particle is given by [2]. Substituting [2], [5] and [6] into [4] yields

$$\frac{dU}{dt} = \frac{2(\rho_p - \rho)}{2\rho_p + \rho}g(1-A)\exp\left(\frac{B}{d}\int_t^{t_c} U\,dt\right) - \frac{18\sqrt{\pi\rho\mu}}{(2\rho_p+\rho)\pi d}\int_0^t \frac{\dfrac{dU}{d\tau}}{\sqrt{t-\tau}}\,d\tau, \quad [7]$$

where t_c is the time when particles become in contact.

Equation [7] can be solved numerically. An analytical solution of [7] for the case of wake attraction, however, can be obtained with some assumptions. The assumptions can be made by considering the following two points: (1) from flow-field visualization for the wake, it can be reasonably assumed that the characteristic length of a wake is 2 particle diameters, i.e. $l_0/d = 2$; and (2) based on the velocity measurements of a particle due to wake attraction, as shown in figure 10, a linear relationship between the velocity of the trailing particle and l/d can be postulated when $l/d < 2$. In the general model formulation, an initial velocity of the trailing particle is given. Based on point (2) above:

$$\frac{dU}{dx} = \frac{dU}{d\left(\dfrac{l}{d}\right)} = -C, \quad [8]$$

where C is a constant which varies with the material properties of both the particle and the fluid; and U is the relative velocity of the trailing particle to the leading particle. Note that $U = -dl/dt$, so that

$$\frac{dU}{dt} = \frac{C}{d}U. \quad [9]$$

Assuming the particle–particle contact velocity at the contact moment t_c is U_c, the time-dependent velocity U can be obtained by integrating [10]:

$$U = U_c\exp\left[-\frac{C}{d}(t_c - t)\right], \quad [10]$$

so that the initial velocity is expressed by

$$U_0 = U_c\exp\left(-\frac{C}{d}t_c\right). \quad [11]$$

Thus, [7] is simplified to

$$CU = \frac{2(\rho_p - \rho)}{2\rho_p + \rho}gd(1-A)\exp\left(\frac{B}{d}\int_t^{t_c} U\,dt\right) - \frac{18U}{2\rho_p+\rho}\sqrt{\frac{C}{d}\rho\mu}\,\mathrm{erf}\left(\sqrt{\frac{C}{d}}t\right), \quad [12]$$

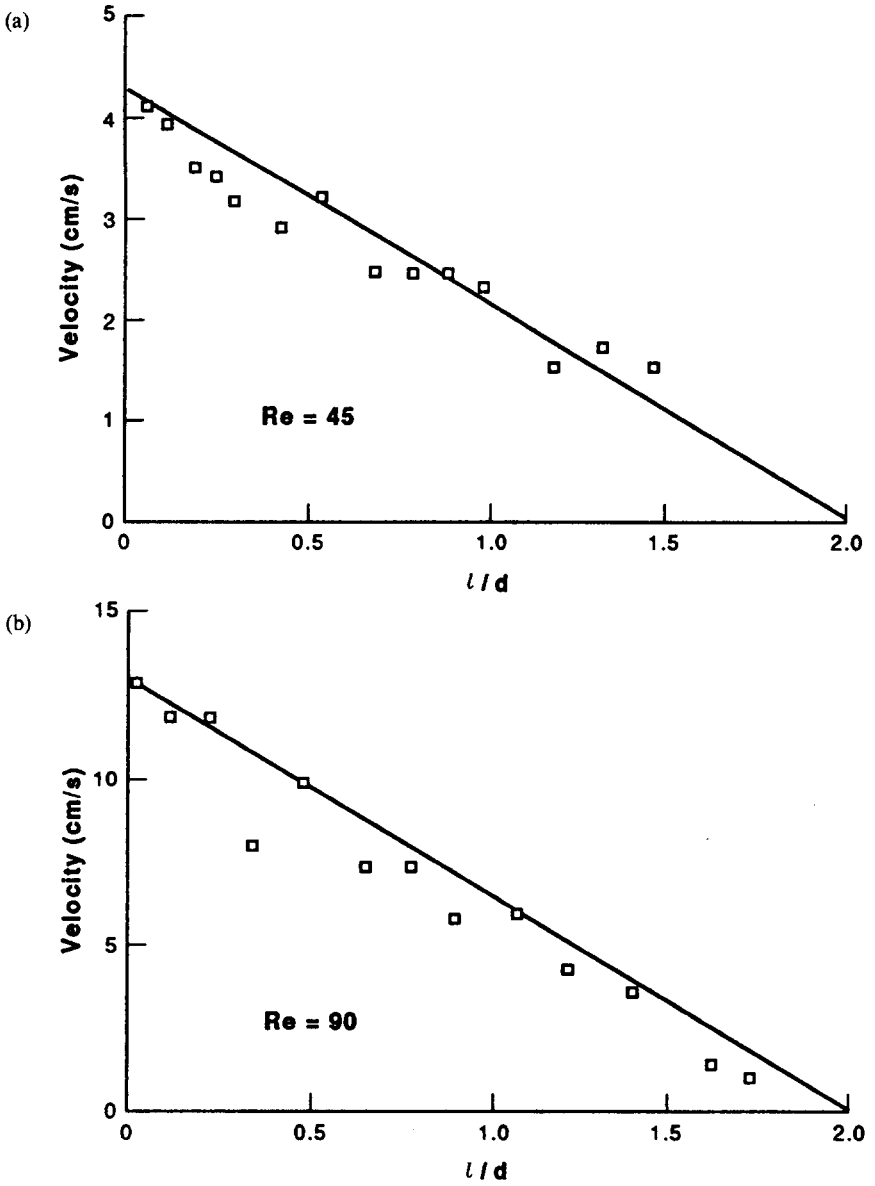

Figure 10. Variation in the velocity of the trailing particle with the interparticle distance during the contacting process: (a) Re = 45; (b) Re = 90.

where erf(x) is the error function of x. At the moment of contact, [12] reduces to

$$\frac{(U_c - U_0)d}{l_0} U_c = \frac{2(\rho_p - \rho)}{2\rho_p + \rho} gd(1 - A) - \frac{18U_c}{2\rho_p + \rho} \sqrt{\frac{U_c - U_0}{l_0} \rho\mu}\, \mathrm{erf}\left[\sqrt{\ln\left(\frac{U_c}{U_0}\right)}\right]; \qquad [13]$$

[13] expressed the contact velocity explicitly as a function of the given flow conditions and the properties of the fluid and particles.

To assess the contributions of the Basset force in the prediction of the particle–particle contact velocity, it is assumed that the Basset force can be neglected and thus [7] becomes

$$-U\frac{dU}{dl} = \frac{2(\rho_p - \rho)}{2\rho_p + \rho} g(1 - A)\exp\left(B\frac{l}{d}\right), \qquad [14]$$

which gives U_c as

$$U_c^2 = U_0^2 + \frac{4(\rho_p - \rho)}{2\rho_p + \rho} gd\left(\frac{1 - A}{-B}\right)\left[1 - \exp\left(\frac{Bl_0}{d}\right)\right]. \qquad [15]$$

Table 1. Comparison of the calculated and experiment U_c values

Particle Reynolds number, Re	90	45
Viscosity, μ (kg/m-s)	0.057	0.054
Particle density, ρ_p (kg/m^3)	1500	1300
Fluid density, ρ (kg/m^3)	1200	1200
Particle diameter, d (m)	0.019	0.019
Characteristic distance, l_0/d	2.0	2.0
Contact velocity between 2 particles, U_c (cm/s) (experimental data)	13.0	4.2
Contact velocity between 2 particles, U_c (cm/s) (without Basset force)	26.1	15.4
Contact velocity between 2 particles, U_c (cm/s) (with Basset force)	14.4	5.2

4.2. Comparison of the experimental results with the predictions

The model is validated by comparing the predicted contact velocity with the experimental data. The validation is illustrated by two examples at different Re. In the experiments, the initial velocity of the trailing particle U_0 is set as zero at $l_0/d = 2$. Table 1 shows the comparison of the experimental results with the model predictions with/without consideration of the Basset term. The results suggest that the Basset force should be included in the formulation concerning the particle motion due to wake attraction.

5. CONCLUSIONS

(1) A microforce measuring system is developed to directly measure the drag force between two particles in the wake-influenced region for Re varying from 20 to 130.
(2) The drag ratio of the trailing particle decreases with decreasing interparticle distance. The particle interaction renders the wake vortex of the leading particle longer than that of a single noninteracting particle.
(3) The Re affects not only the magnitude of the drag ratio but also its variation with the interparticle distance. It is possible that the wake-influenced region of the leading particle is shorter at higher Re.
(4) The influence of the leading particle on the drag force of the trailing particle is significantly larger than that of the trailing particle on the leading particle.
(5) A simple mechanistic model is developed to account for the accelerating motion of the trailing particle due to wake attraction. It is found that the Basset force term is important in the model equation and, thus, should be included in the formulation.

Acknowledgement—The work was sponsored by NSF Grant CTS-9200793.

REFERENCES

CLIFT, R., GRACE, J. R. & WEBER, M. E. 1978 *Bubbles, Drops, and Particles*. Academic Press, New York.

HAPPEL, J. & BRENNER, H. 1965 *Low Reynolds Number Hydrodynamics*. Prentice-Hall, Englewood Cliffs, NJ.

JOSEPH, D. 1993 Finite size effects in fluidized suspension experiments. In *Particulate Two-phase Flow* (Edited by ROCO, M. C.), Chap. 10, pp. 300–324. Butterworth-Heineman, London.

LEE, K. C. 1979 Aerodynamic interaction between two spheres at Reynolds numbers around 10^4. *Aerosp. Q.* **30,** 371–385.

ODAR, F. & HAMILTON, W. S. 1964 Forces on a sphere accelerating in a viscous fluid. *J. Fluid Mech.* **18,** 302–314.

ROWE, P. N. & HENWOOD, G. A. 1961 Drag forces in a hydraulic model of a fluidised bed—part I. *Trans. Instn Chem. Engrs* **39,** 43–54.

SCHLICHTING, H. 1979 *Boundary Layer Theory*. McGraw-Hill, New York.

STIMSON, M. & JEFFERY, G. B. 1926 The motion of two spheres in a viscous fluid. *Proc. R. Soc. Lond.* **A111,** 110–116.

TANEDA, S. 1956 Experimental investigation of the wake behind a sphere at low Reynolds numbers. *J. Phys. Soc. Japan* **11,** 1104–1108.

TANEDA, S. 1979 Visualization of separating Stokes flows *J. Phys. Soc. Japan* **46,** 1935–1942.

TSUJI, Y., MORIKAWA, Y. & TERASHIMA, K. 1982 Fluid-dynamic interaction between two spheres. *Int. J. Multiphase Flow* **8**, 71–82.